Science Advances
AAAS

Supplementary Materials for

Macrophage fusion event as one prerequisite for inorganic nanoparticle-induced antitumor response

Siyu Chen *et al.*

Corresponding author: Xiao Yang, xiaoyang114@foxmail.com; Xiangdong Zhu, zhu_xd1973@scu.edu.cn

Sci. Adv. **9**, eadd9871 (2023)
DOI: 10.1126/sciadv.add9871

This PDF file includes:

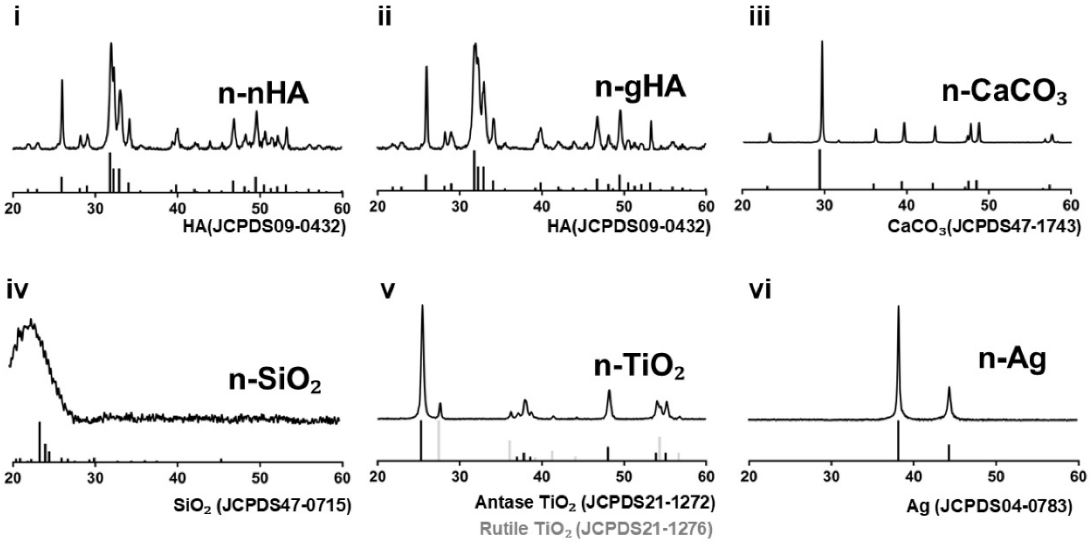

Fig. S1. Nanoparticle characterization (part 1). X-ray diffraction (XRD) patterns of (i) n-nHA, (ii) n-gHA, (iii) n-$CaCO_3$, (iv) n-SiO_2, (v) n-TiO_2 and (vi) n-Ag. The standard patterns are provided below.

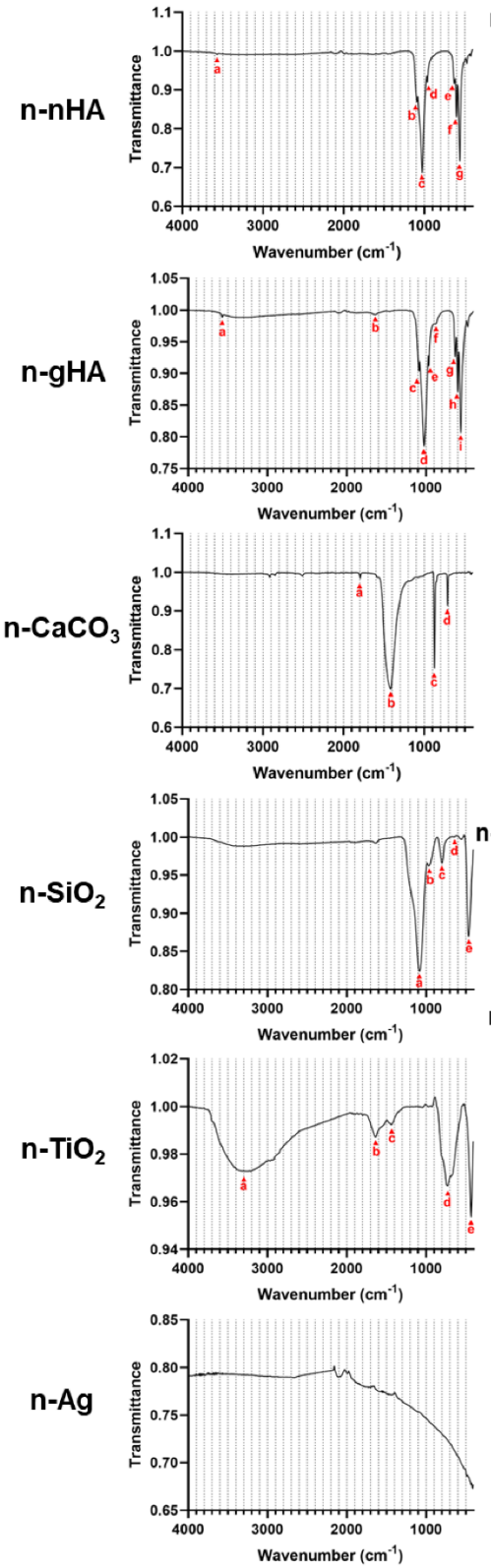

n-nHA

	Peak position (cm^{-1})	Assignment
a	3572 (sharp)	stretching vibration of O-H
b	1090 (shoulder)	Antisymmetriuc stretching of PO_4^{3-}
c	1040 (sharp)	Antisymmetriuc stretching of PO_4^{3-}
d	962 (shoulder)	$_{v1}PO_4^{3-}$
e	615 (shoulder)	$_{v4}PO_4^{3-}$
f	602 (shoulder)	$_{v4}PO_4^{3-}$
g	569 (sharp)	$_{v4}PO_4^{3-}$

n-gHA

	Peak position (cm^{-1})	Assignment
a	3572 (sharp)	stretching vibration of O-H
b	1634	δ-H_2O bending + vibrations of hydroxyl groups
c	1090 (shoulder)	Antisymmetriuc stretching of PO_4^{3-}
d	1040 (sharp)	Antisymmetriuc stretching of PO_4^{3-}
e	962 (shoulder)	$_{v1}PO_4^{3-}$
f	875 (shoulder)	Vibration of carbonate group
g	615 (shoulder)	$_{v4}PO_4^{3-}$
h	602 (shoulder)	$_{v4}PO_4^{3-}$
i	569 (sharp)	$_{v4}PO_4^{3-}$

$n-CaCO_3$

	Peak position (cm^{-1})	Assignment
a	1420 (broad and sharp)	Asymmetric stretching of carbonate group
b	870 (sharp)	Out-of-plane bending of carbonate group
c	460-480 (sharp)	In-plane bending of carbonate group

$n-SiO_2$

	Peak position (cm^{-1})	Assignment
a	1050-1060 (broad and sharp)	Antisymmetriuc stretching + vibrations of bridging oxygens
b	960 (shoulder)	Vibration of nonbridging oxygens
c	775-800 (sharp)	Symmetric stretching vibration of [O–Si–O] bonds
d	640-680 (shoulder)	Si–O–Si and O–Si–O bending modes
e	460-480 (very sharp)	Bending vibrations of Si–O–Si linkages

$n-TiO_2$

	Peak position (cm^{-1})	Assignment
a	3300 (broad)	δ-H_2O bending + vibrations of hydroxyl groups
b	1640 (sharp)	δ-H_2O bending + vibrations of hydroxyl groups
c	1430 (shoulder)	vibration of C–H
d	732 (broad)	stretching vibration of O–Ti–O bonding
e	450 (very sharp)	Bending vibrations of O–Ti–O linkages

Fig. S2. Nanoparticle characterization (part 2). Fourier transform infrared spectroscopy (FTIR) spectra of (i) n-nHA, (ii) n-gHA, (iii) n-$CaCO_3$, (iv) n-SiO_2, (v) n-TiO_2 and (vi) n-Ag. The characteristic peaks and corresponding assignments are provided on the left. Because n-Ag is black, no characteristic peak is detected by FTIR.

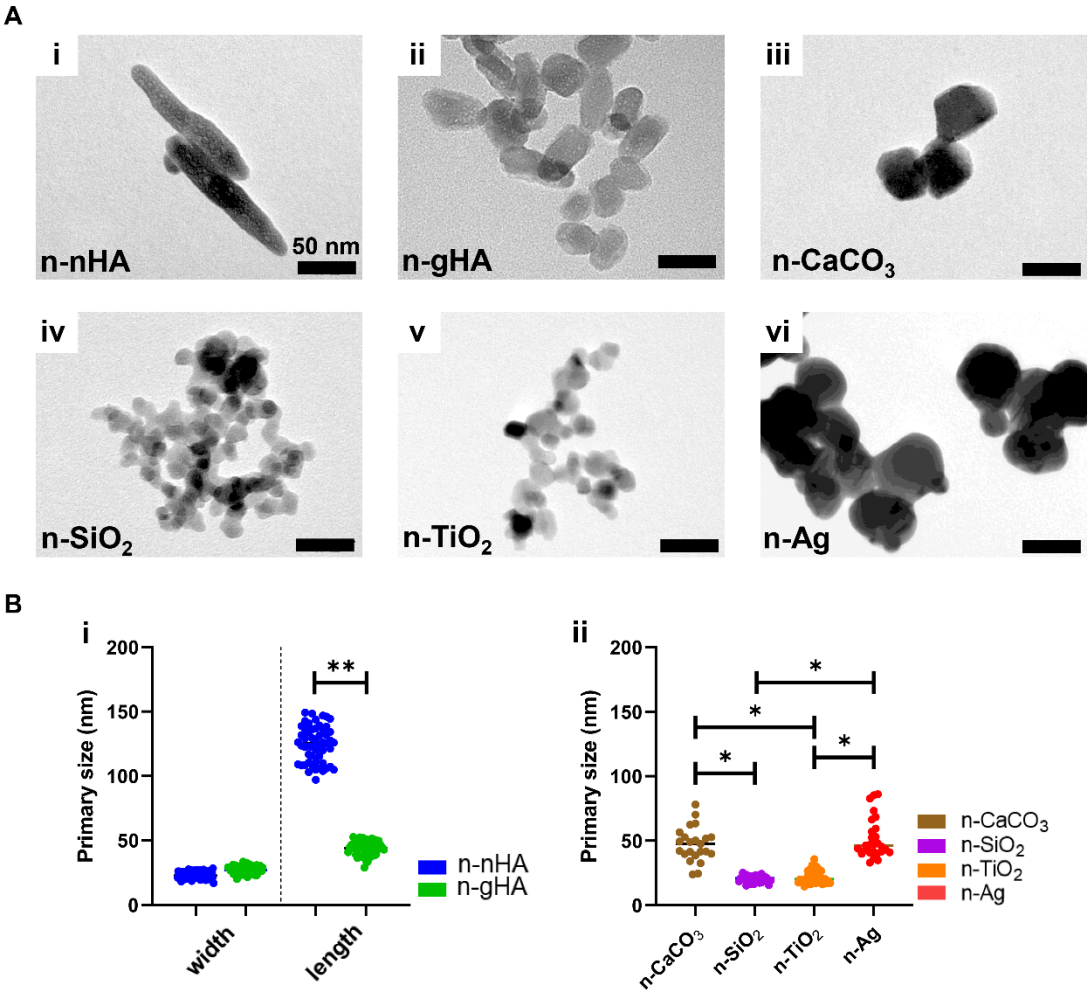

Fig. S3. Nanoparticle characterization (part 3). (**A**) Representative transmission electron microscope (TEM) images of (i) n-nHA, (ii) n-gHA, (iii) n-$CaCO_3$, (iv) n-SiO_2, (v) n-TiO_2 and (vi) n-Ag. Scale bars, 50 nm. (**B**) Measurement of nanoparticle primary sizes obtained from TEM images. *$P < 0.05$, **$P < 0.01$.

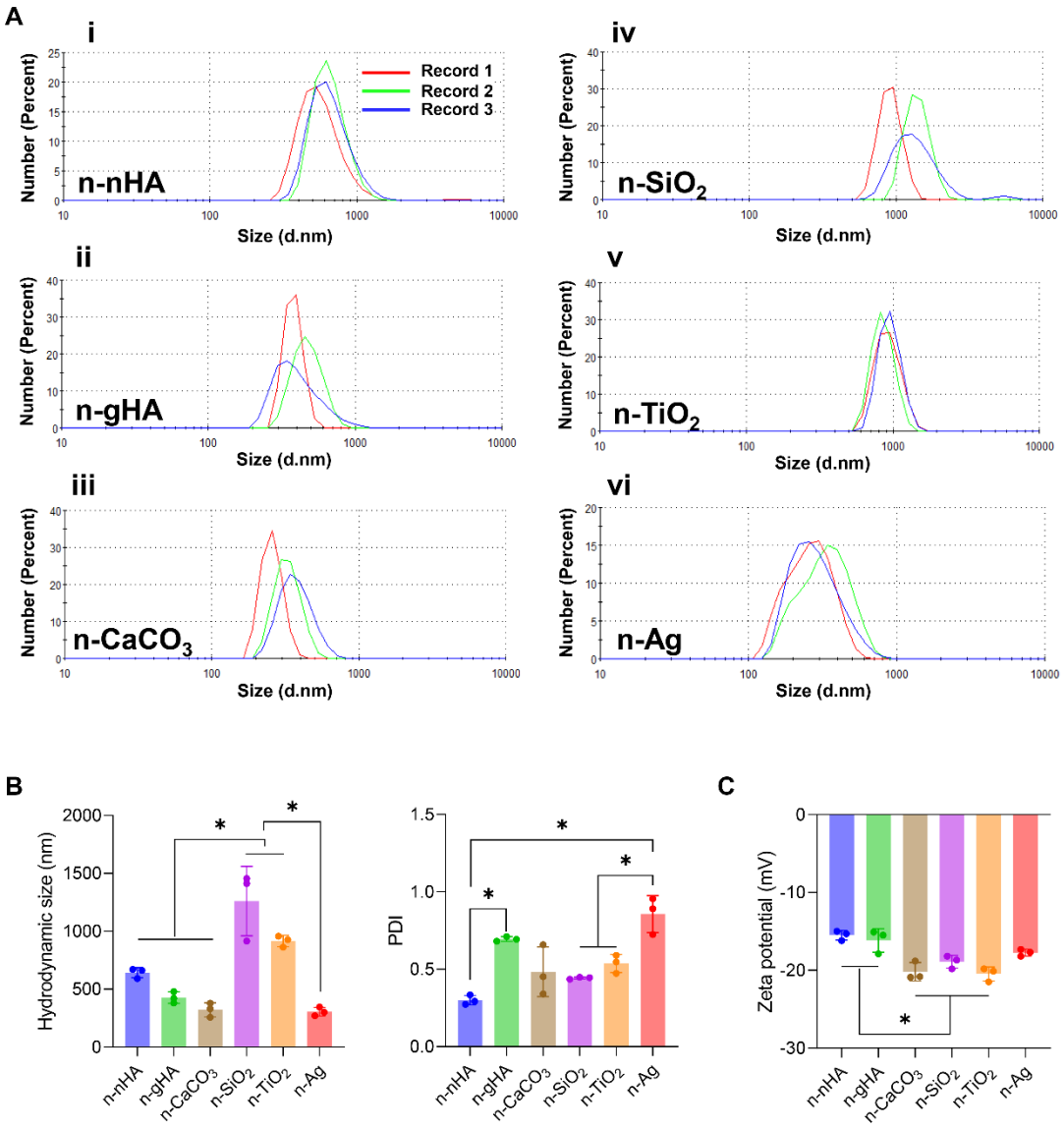

Fig. S4. Nanoparticle characterization (part 4). (**A**) The distribution of hydrodynamic size: (i) n-nHA, (ii) n-gHA, (iii) n-$CaCO_3$, (iv) n-SiO_2, (v) n-TiO_2 and (vi) n-Ag obtained by dynamic light scattering. (**B**) The average hydrodynamic sizes and particle dispersion index (PDI) values of different nanoparticles. (**C**) Zeta potentials of different nanoparticles. *$P < 0.05$.

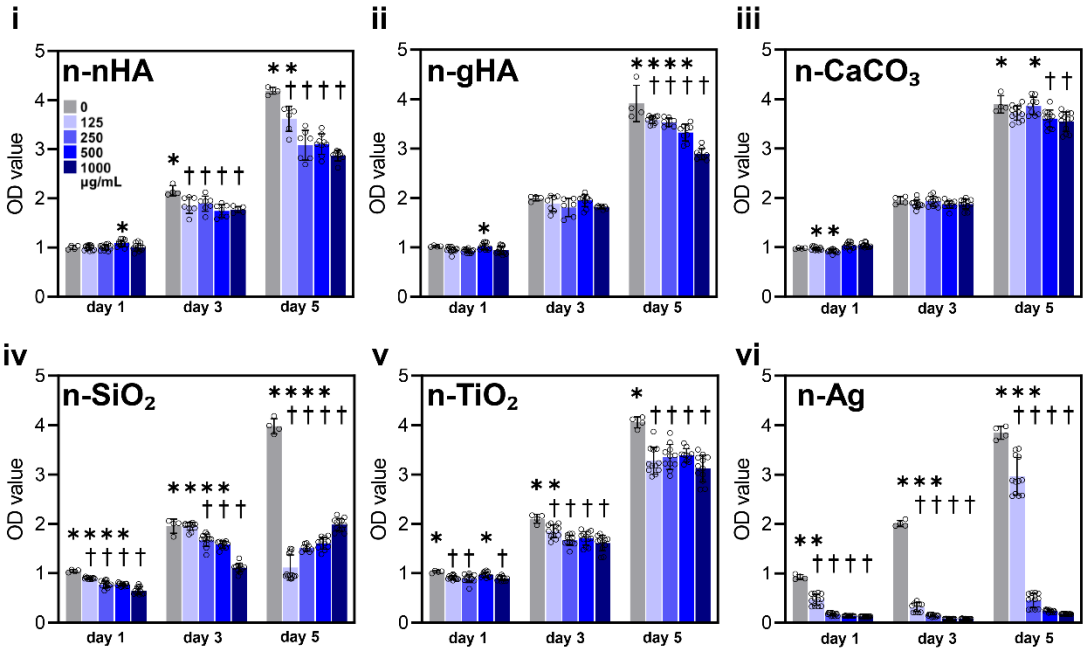

Fig. S5. Cytotoxicity assay of inorganic nanoparticles. Proliferation of 4T1 tumor cells cocultured with 0, 125, 250, 500, 1000 μg/mL n-nHA (i), n-gHA (ii), n-$CaCO_3$ (iii), n-SiO_2 (iv), n-TiO_2 (v) and n-Ag (vi) for 1, 3 and 5 days, determined by CCK-8 assay. * $P < 0.05$ compared to 1000 μg/mL, † $P < 0.05$ compared to 0 μg/mL, significant difference was assessed by one-way analysis of variance followed by Tukey's post hoc test.

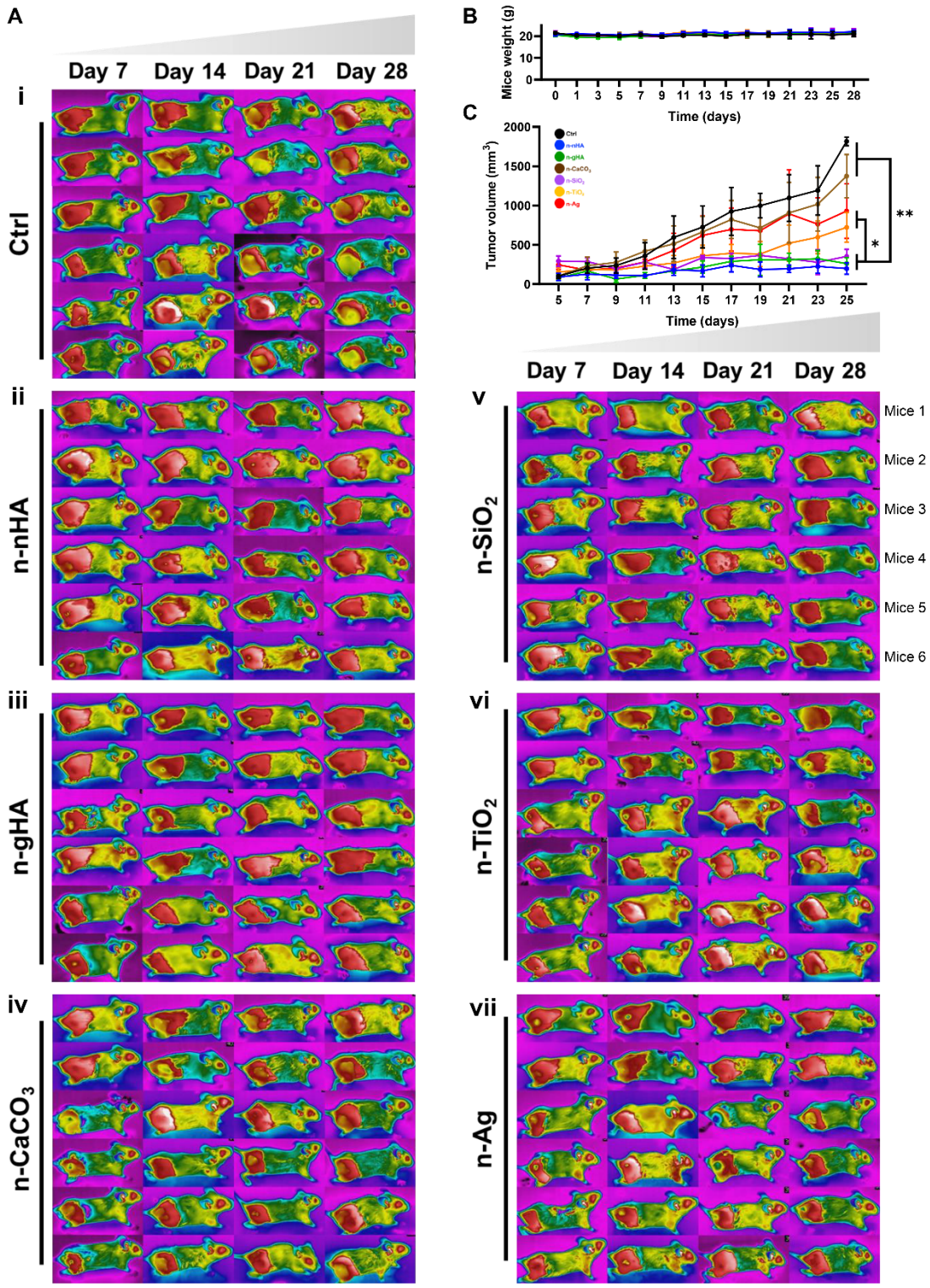

Fig. S6. Routine observation of tumor-beraing mice with different nanoparticle treatments. (**A**) Representative thermal images of tumor-bearing mice after nanoparticle treatments from day 7 to day 28. (**B**) Body weight and (**C**) tumor volumes of tumor-bearing mice treated with different nanoparticles. $^{*}P < 0.05$, $^{*}P < 0.01$, significant difference was assessed by one-way analysis of variance followed by Tukey's post hoc test.

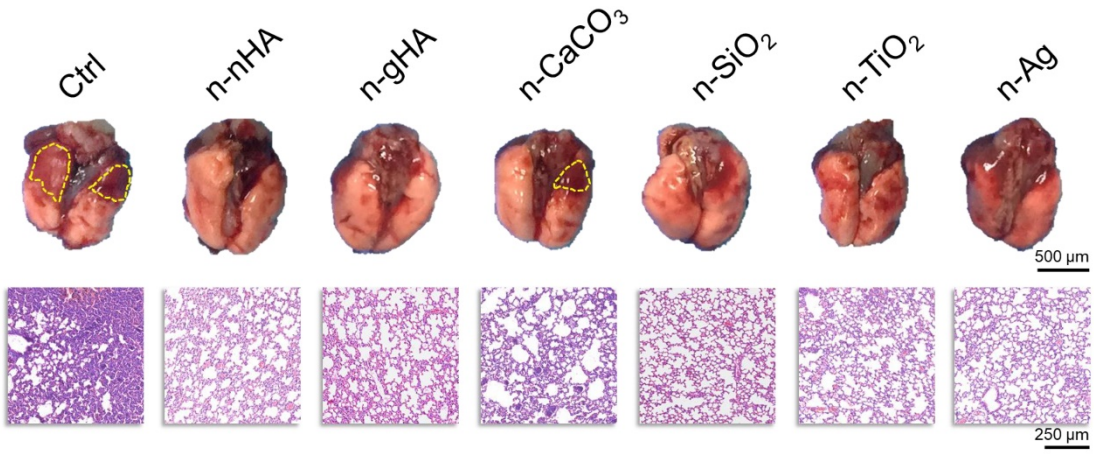

Fig. S7. Observation of lung tissues of tumor-bearing mice. Representative lung images (upper row) of different groups. Lung metastases are indicated within yellow dotted lines. Scale bar, 500 μm. The corresponding H&E staining images (bottom row) of lung tissues. Scale bar, 250 μm.

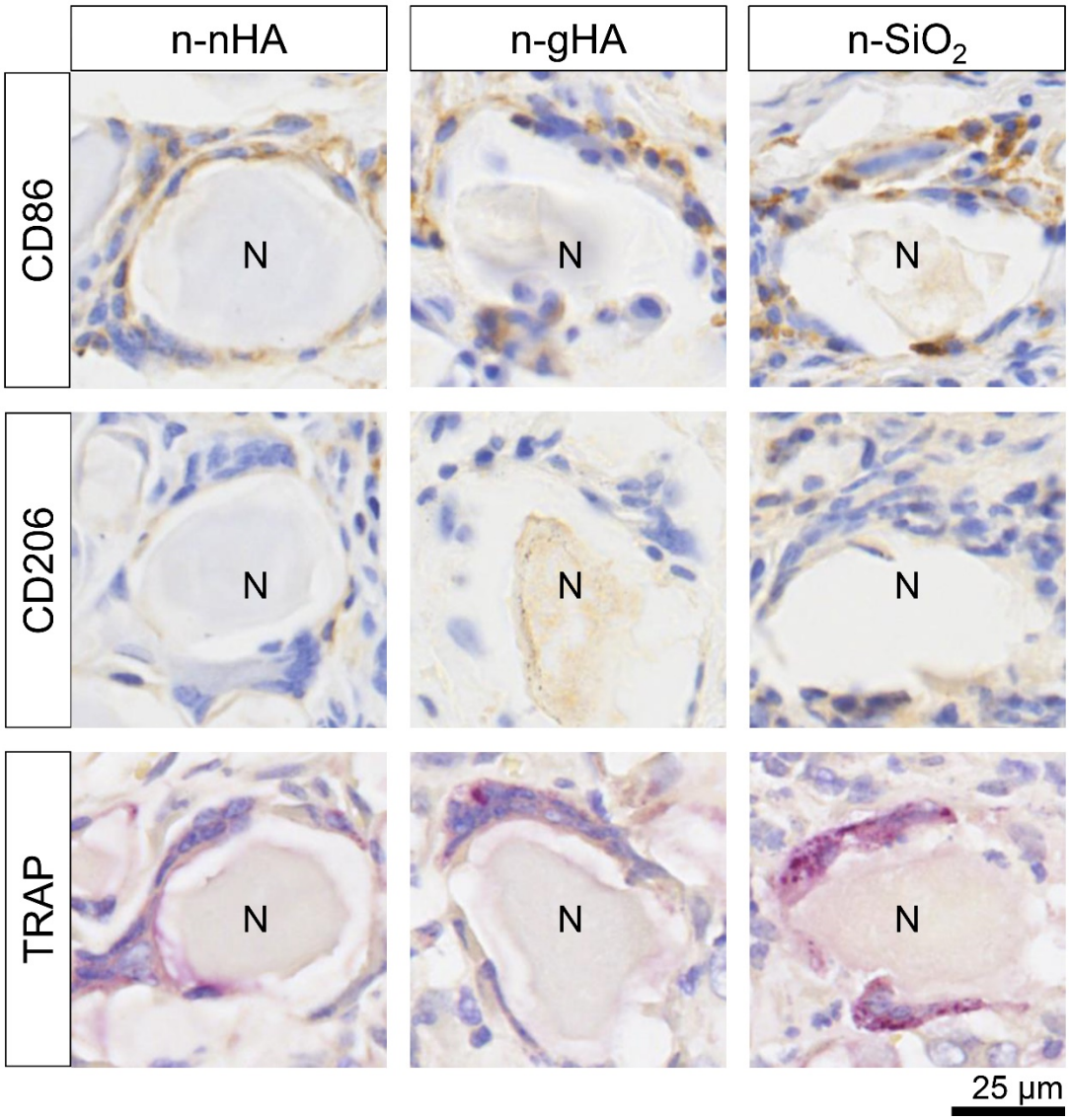

Fig. S8. Immunohistochemistry (IHC) analysis of multinucleated giant cells (MNGCs). Representative IHC images for MNGCs marked by $CD86^{high}$, $CD206^{low}$ and $Trap^{high}$. Scale bar, 25 μm. N, aggregates of nanoparticles.

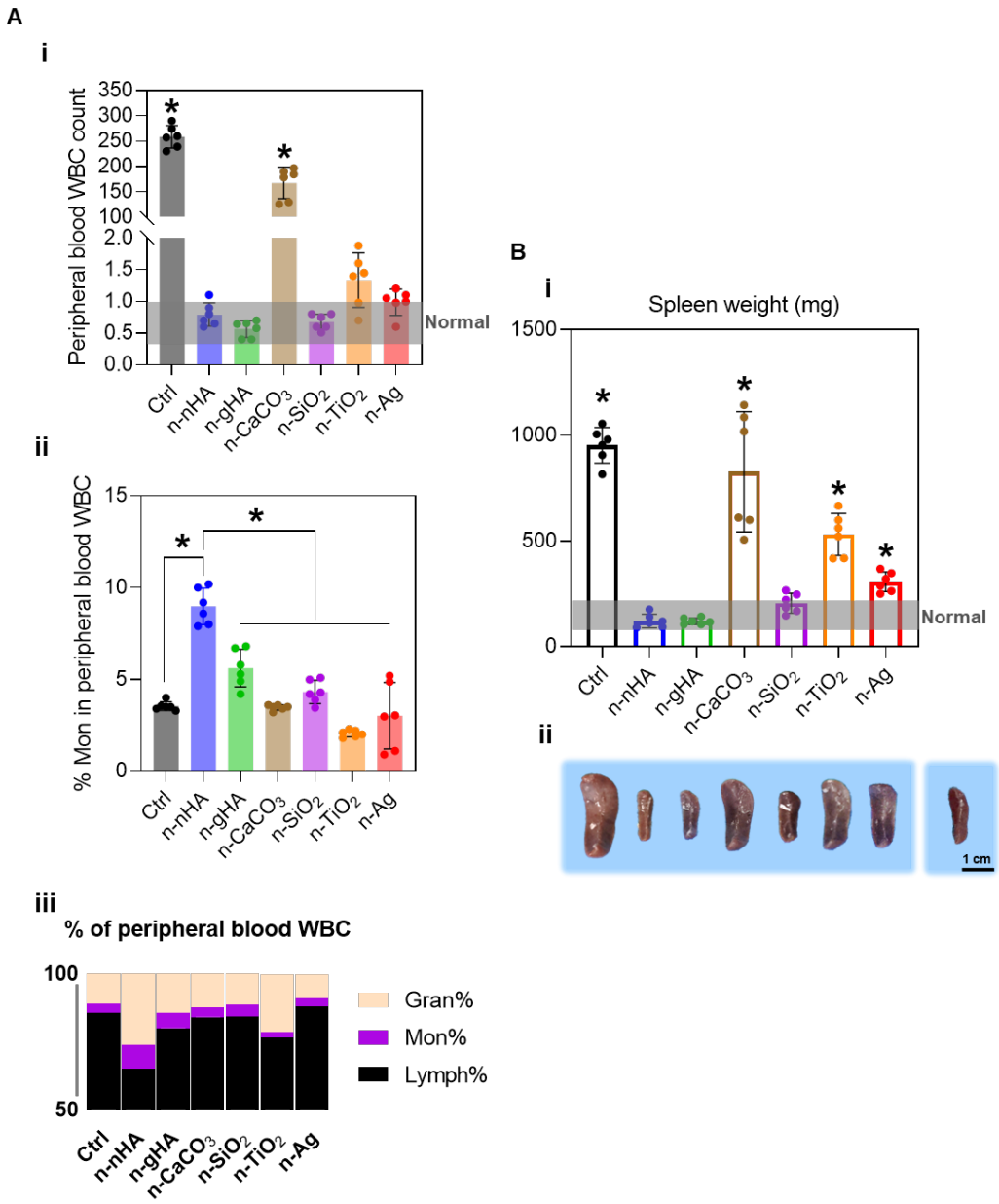

Fig. S9. Observation of blood and spleen tissues of tumor-bearing mice. (**A**) Leucocyte counts in the peripheral blood of tumor-bearing mice after nanoparticle treatments for 28 days. (**B**) Weight (i) and representative images (ii) of mouse spleens after nanoparticle treatments for 28 days. Scale bar, 1 cm. *$P < 0.05$, significant difference was assessed by one-way analysis of variance followed by Tukey's post hoc test, compared to n-nHA, n-gHA and n-SiO_2 groups.

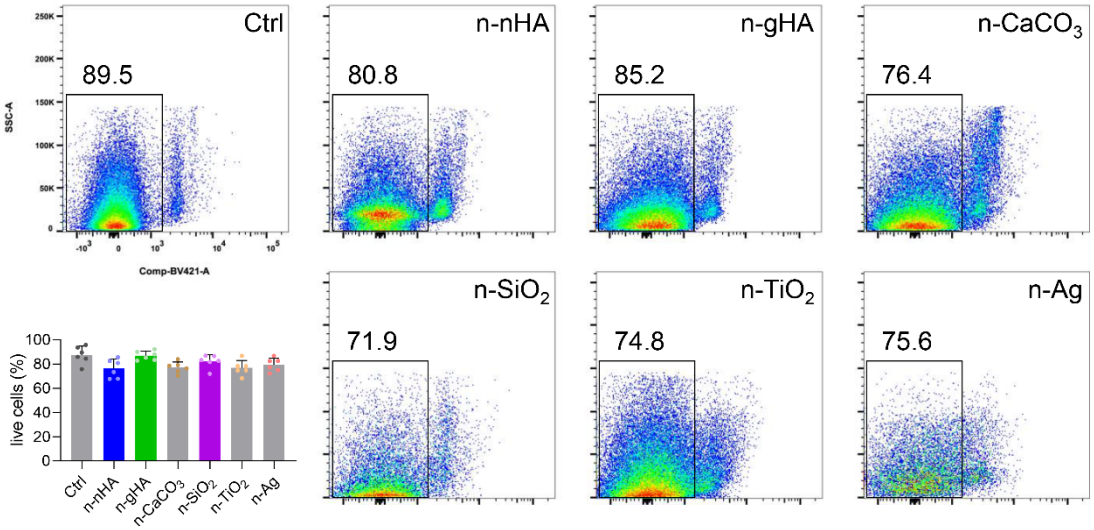

Fig. S10. Live cells in the mouse tumors treated with different nanoparticles. Representative scatter plots and quantification of live cells in the tumors excised at day 28.

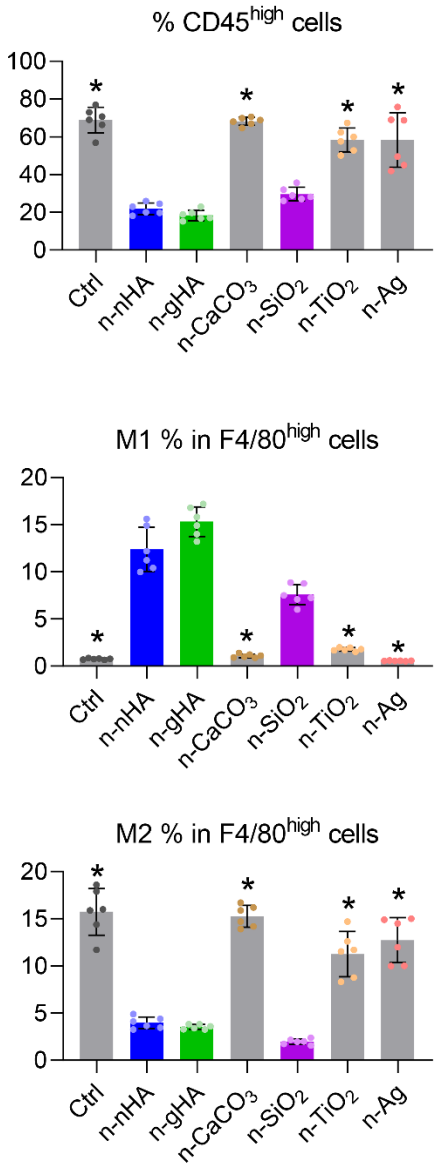

Fig. S11. Quantification of total lymphocytes and macrophages in the mouse tumors. Quantification of $CD45^{high}$ lymphocytes, $CD86^{high}$ M1-like macrophages and $CD206^{high}$ M2-like tumor-associated macrophages in the tumors excised at day 28. $^{*}P < 0.05$, significant difference was assessed by one-way analysis of variance followed by Tukey's post hoc test, compared to n-nHA, n-gHA and n-SiO_2 groups.

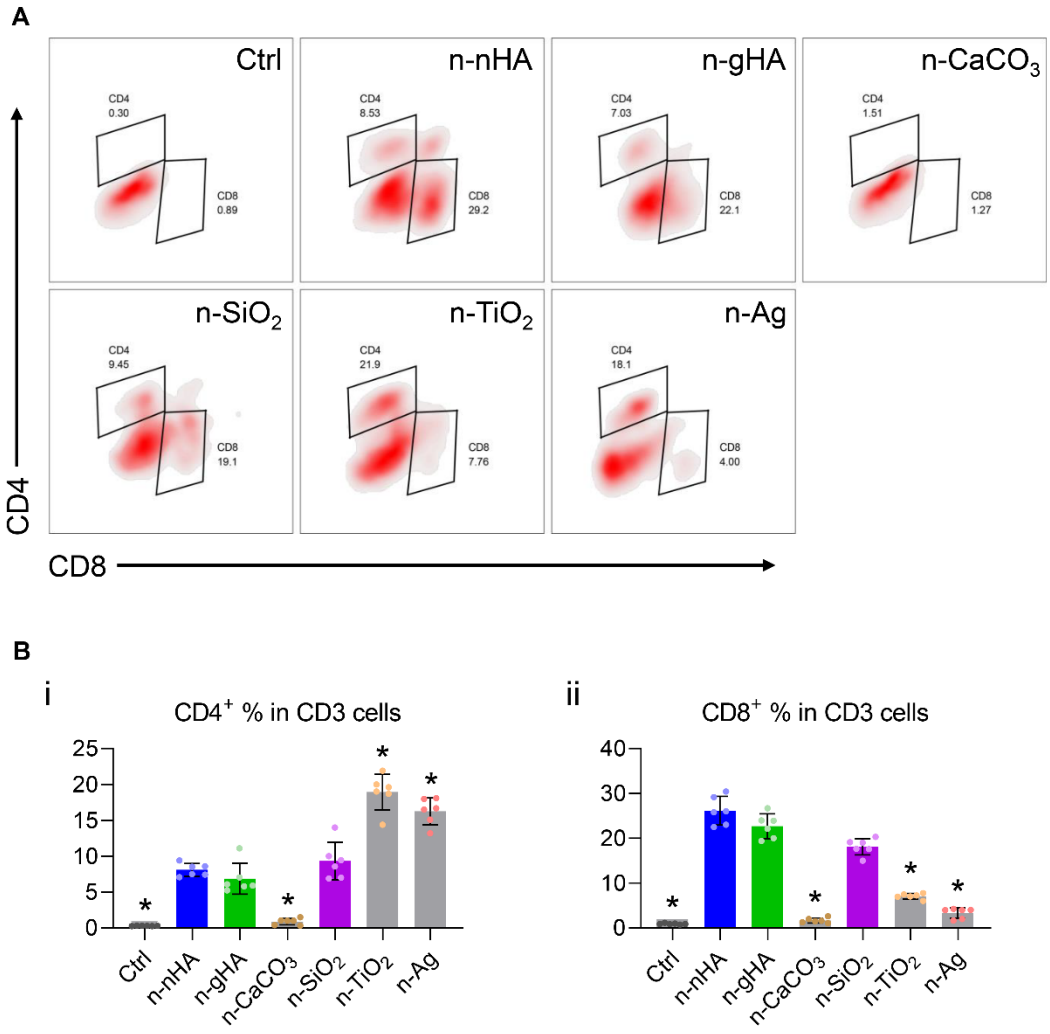

Fig. S12. Local immune constitution of T-cell clusters in the tumor microenvironment of mice treated with different nanoparticles. (**A**) Representative scatter plots and (**B**) quantification of $CD3^{high}CD4^{high}$ T cells (i) and $CD3^{high}CD8^{high}$ T cells (ii) in the tumors excised at day 28. **P* < 0.05, significant difference was assessed by one-way analysis of variance followed by Tukey's post hoc test, compared to n-nHA, n-gHA and n-SiO_2 groups.

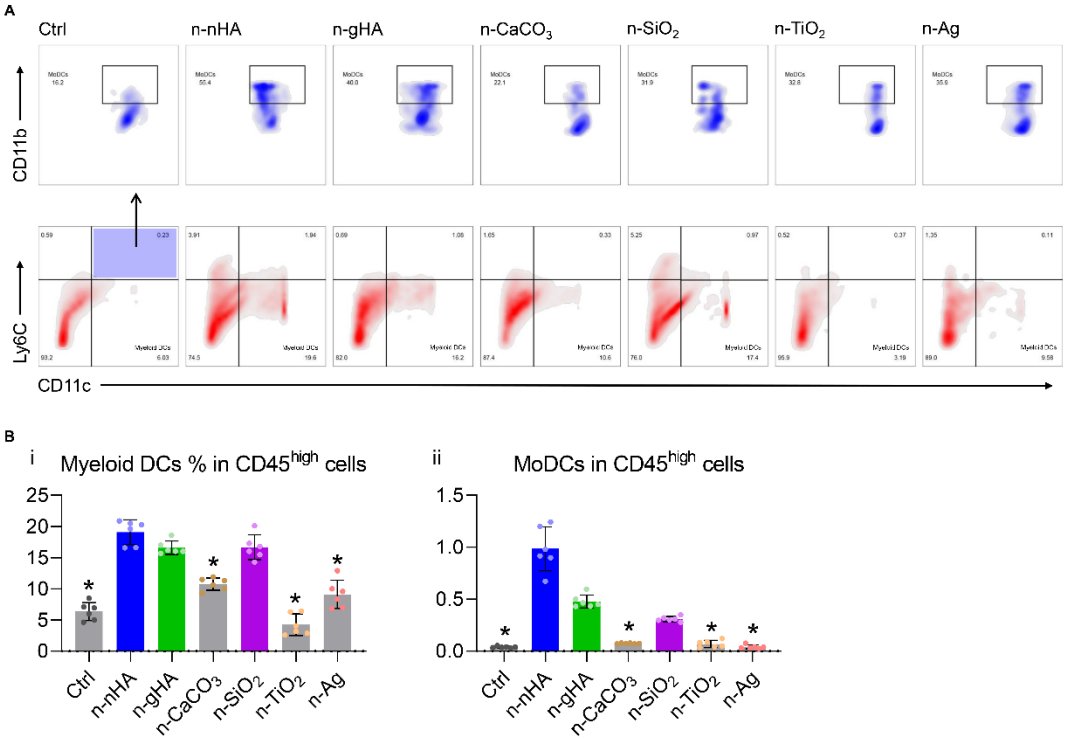

Fig. S13. Local immune constitution of dendritic cell (DC) clusters in the tumor microenvironment of mice treated with different nanoparticles. (**A**) Representative scatter plots of Ly6C^{low}CD11c^{high} myeloid DCs (blue, bottom row) and Ly6C^{high}CD11c^{high}CD11b^{high} monocyte-derived dendritic cells (MoDCs) (red, upper row) in the tumors excised at day 28. (**B**) The corresponding quantification of myeloid DCs (i) and MoDCs (ii). *$P < 0.05$, significant difference was assessed by one-way analysis of variance followed by Tukey's post hoc test, compared to n-nHA, n-gHA and n-SiO_2 groups.

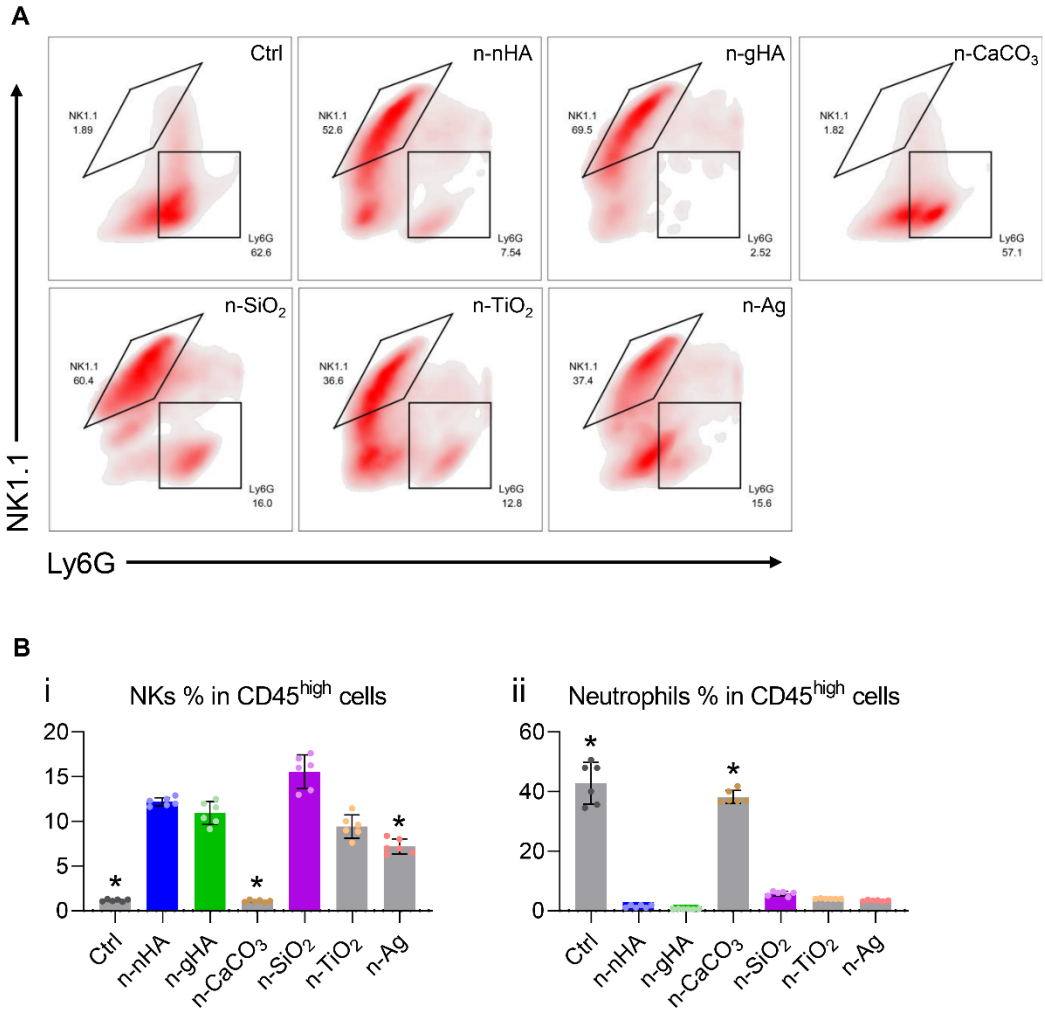

Fig. S14. Local immune constitution of natural killer cells (NKs) and neutrophils in the tumor microenvironment of mice treated with different nanoparticles. (**A**) Representative scatter plots and (**B**) quantification of $CD45^{high}Ly6G^{low}NK1.1^{high}$ NKs (i) and $CD45^{high}Ly6G^{high}$ neutrophils (ii) in the tumors excised at day 28. **P* < 0.05, significant difference was assessed by one-way analysis of variance followed by Tukey's post hoc test, compared to n-nHA, n-gHA and n-SiO_2 groups.

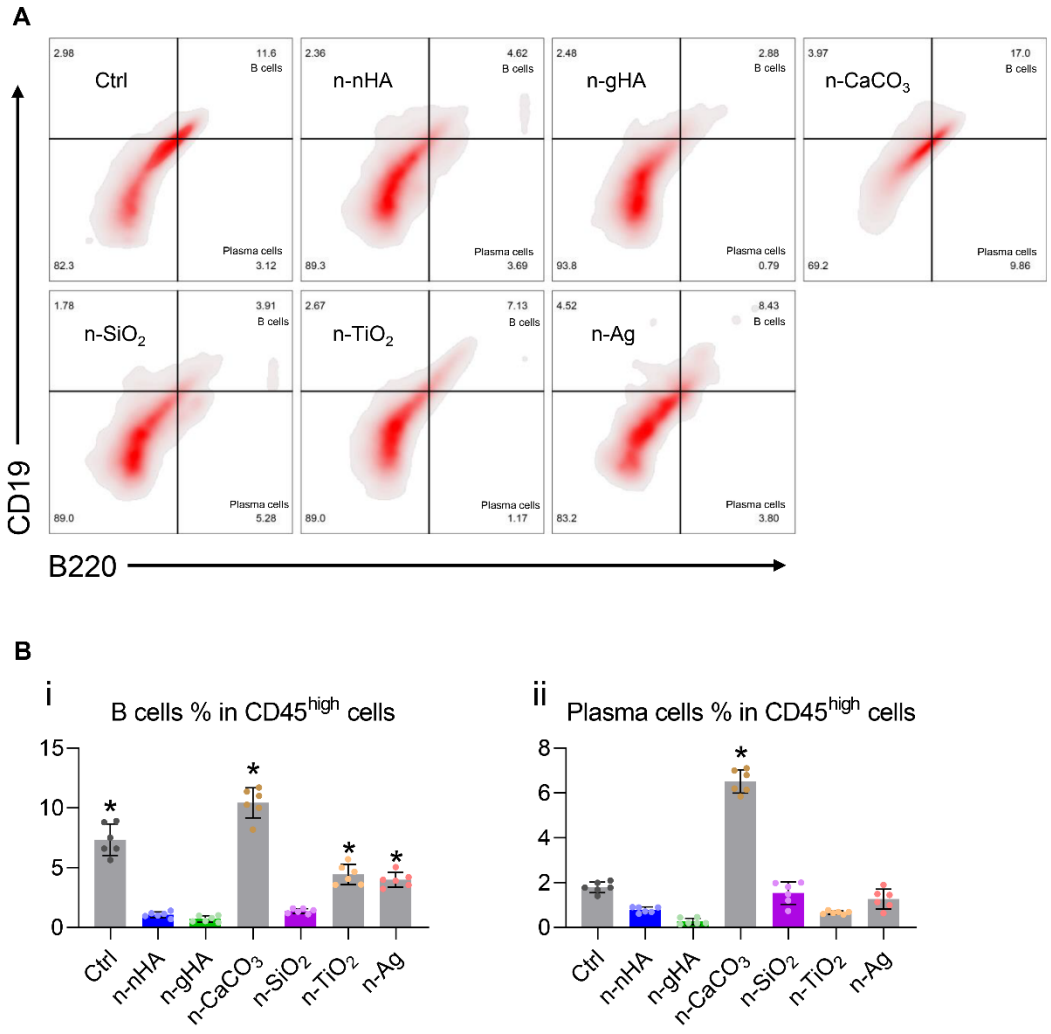

Fig. S15. Local immune constitution of the B-cell cluster in the tumor microenvironment of mice treated with different nanoparticles. (**A**) Representative scatter plots and (**B**) quantification of $B220^{high}CD19^{high}$ B cells (i) and $B220^{high}CD19^{low}$ plasma cells (ii) in the tumors excised at day 28. $^{*}P < 0.05$, significant difference was assessed by one-way analysis of variance followed by Tukey's post hoc test, compared to n-nHA, n-gHA and n-SiO_2 groups.

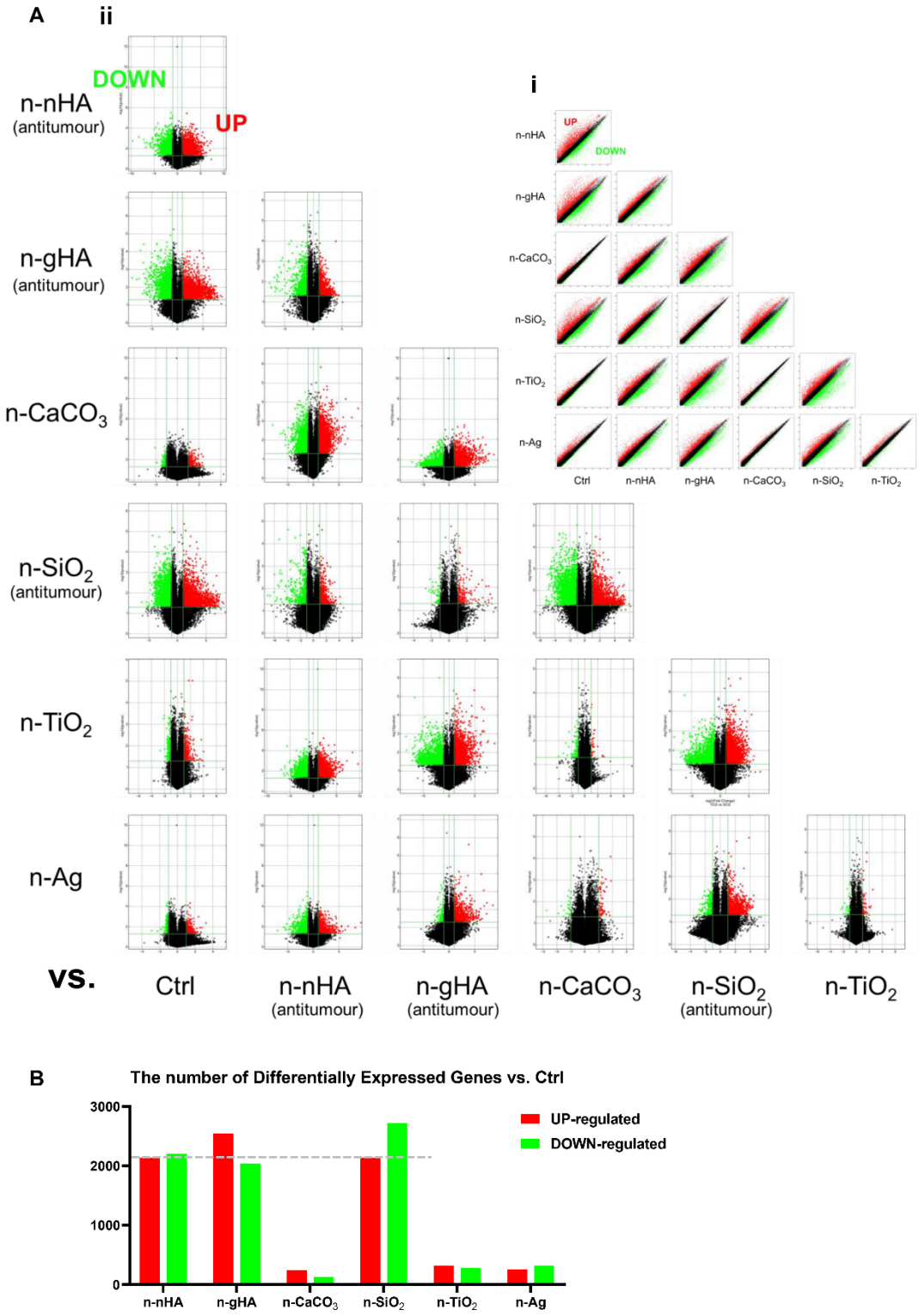

Fig. S16. Differentially expressed genes detected in n-nHA, n-gHA and n-SiO_2 (antitumor groups) compared to other ineffective groups. (**A**) Scatter plots (i) of differentially expressed genes (fold-change > 2) and volcano plots (ii) of differentially expressed genes ($P < 0.05$, fold-change > 2), comparing every two groups. (**B**) The number of differentially expressed genes in all nanoparticle groups compared to the Ctrl group.

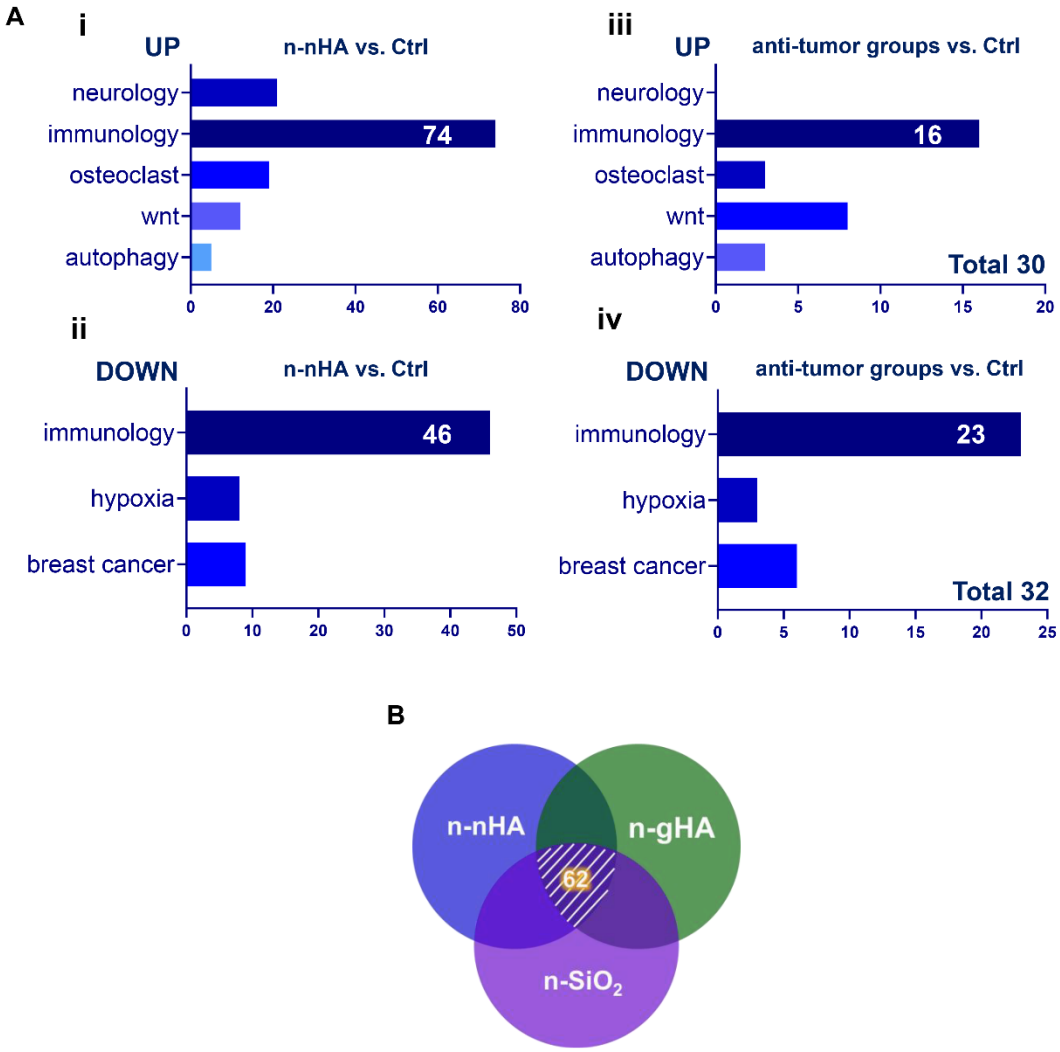

Fig. S17. Differentially expressed genes participating in the antitumor immunity of n-nHA, n-gHA and n-SiO_2 (antitumor groups). (**A**) The number and category of differentially expressed genes. (**B**) Venn diagram showing 62 overlapping genes across n-nHA, n-gHA and n-SiO_2 compared with Ctrl.

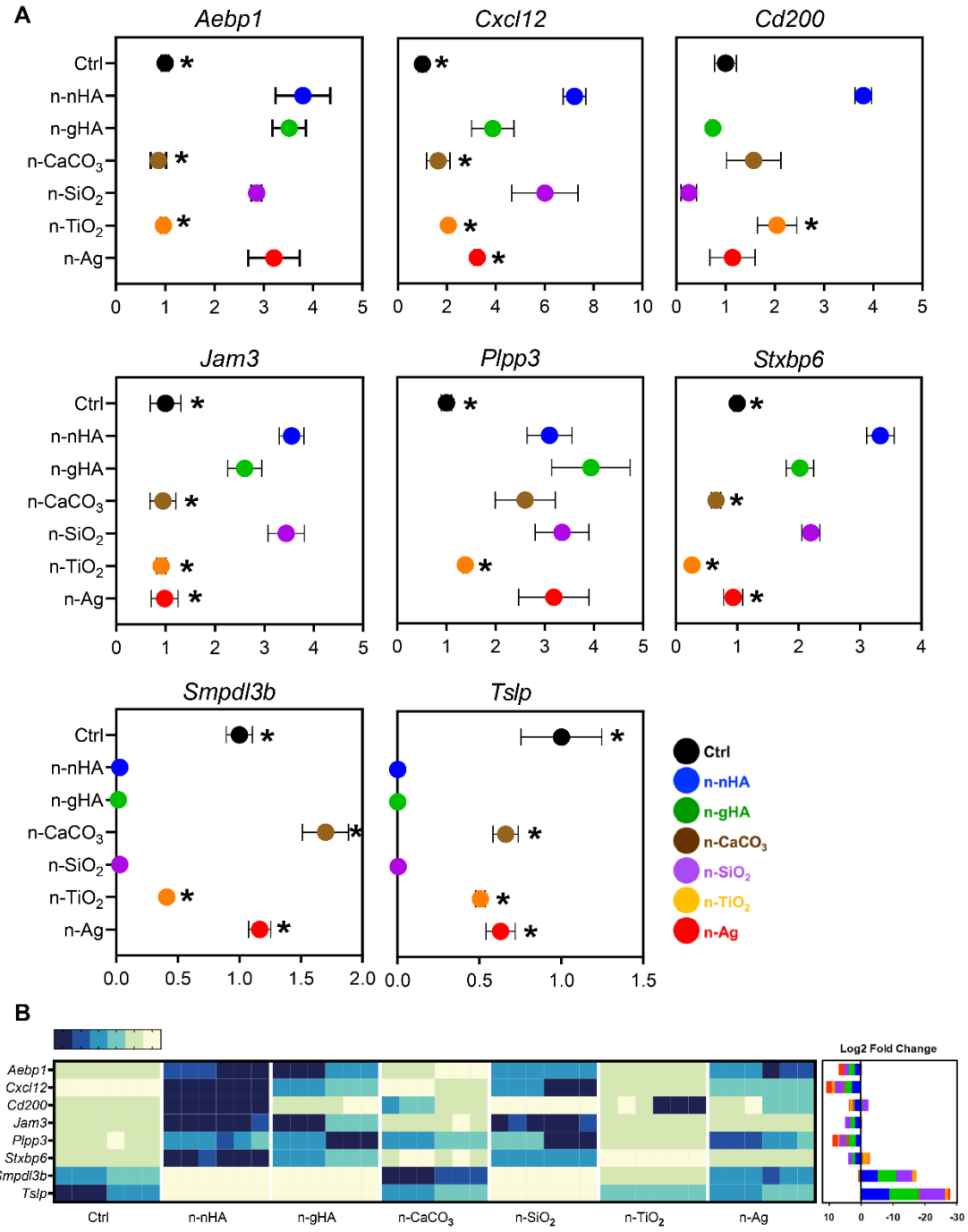

Fig. S18. Quantitative real-time polymerase chain reaction (qPCR) analysis applied for assessing the expression of the eight selected genes from principal component analysis (PCA) at the mRNA level. (**A**) Quantification of the gene expression of *Aebp1*, *Cxcl12*, *Cd200*, *Jam3*, *Plpp3*, *Stxbp6*, *Smpdl3b* and *Tslp* in mouse tumor samples. Mouse *Gapdh* was used as a housekeeping gene. **P* < 0.05, significant difference was assessed by one-way analysis of variance followed by Tukey's post hoc test, compared to n-nHA, n-gHA and n-SiO_2 groups. (**B**) Heatmap (left) of the gene expression of *Aebp1*, *Cxcl12*, *Cd200*, *Jam3*, *Plpp3*, *Stxbp6*, *Smpdl3b* and *Tslp* in all groups, row normalized to each gene's maximum positive expression. Stacked bar plot (right) of the $\log_2$ fold change in gene expression, colored by nanoparticles.

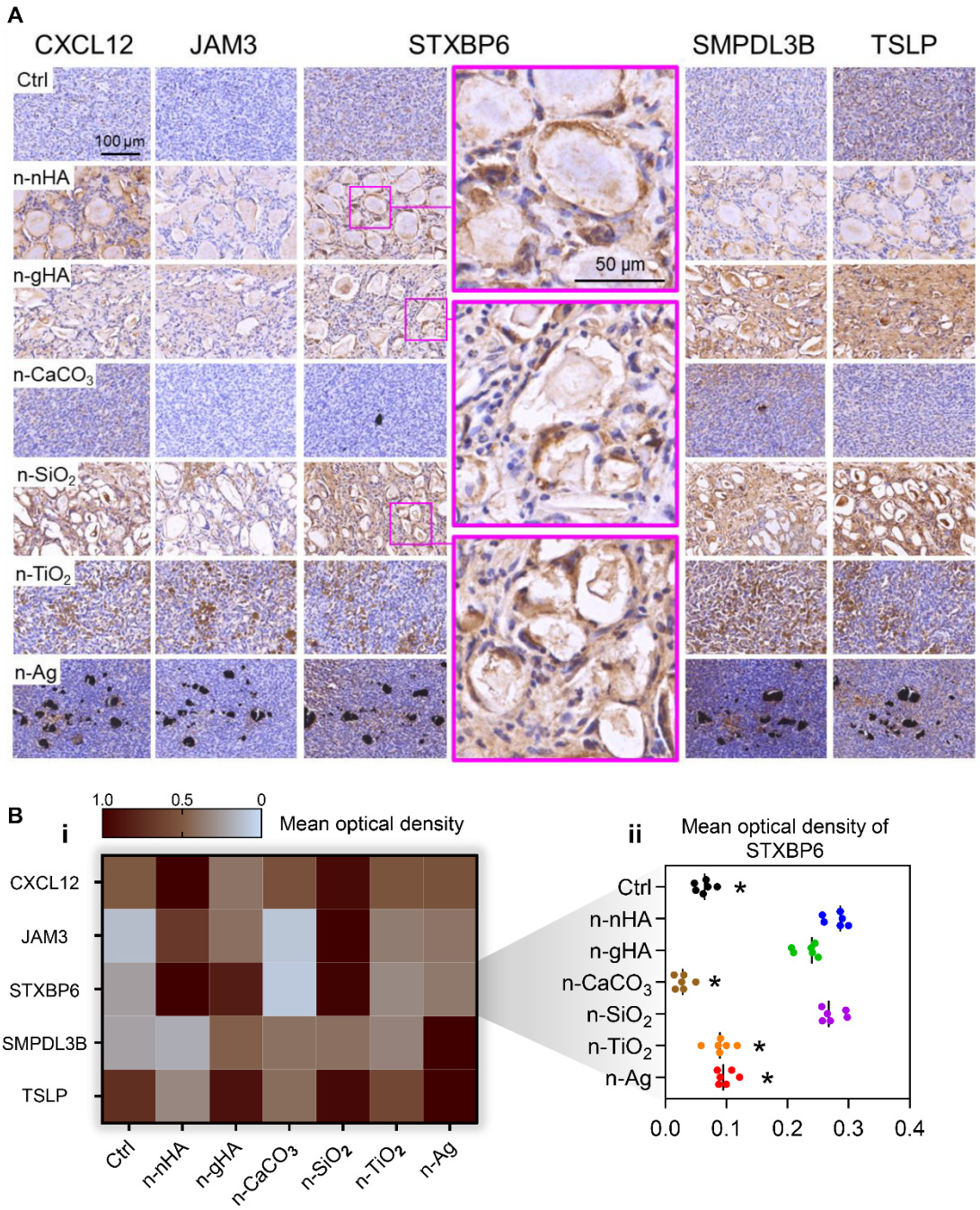

Fig. S19. Immunohistochemistry (IHC) analyses show that STXBP6 was specifically expressed in MNGCs of the n-nHA, n-gHA and n-SiO_2 groups (antitumor groups). (**A**) Representative IHC images of CXCL12, JAM3, STXBP6, SMPDL3B and TSLP in tumor tissues treated with different nanoparticles at day 28. Scale bar, 100 μm. Scale bar of the magnified IHC images of STXBP6, 50 μm. (**B**) Heatmap (i) of the mean optical density of CXCL12, JAM3, STXBP6, SMPDL3B and TSLP from IHC images, row normalized to each protein's maximum positive expression. Quantification (ii) of STXBP6 expression. **P* < 0.05, significant difference was assessed by one-way analysis of variance followed by Tukey's post hoc test, compared to n-nHA, n-gHA and n-SiO_2 groups.

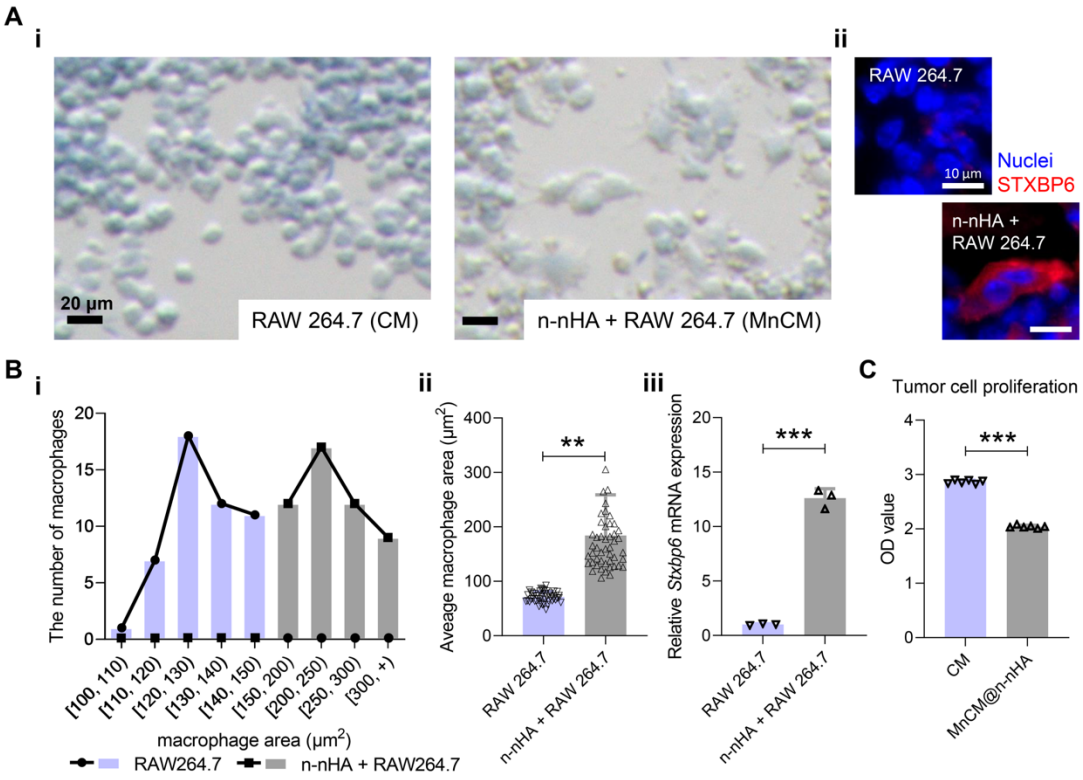

Fig. S20. RAW 264.7 macrophages cocultured with n-nHA. (**A**) Representative photographs (i) and immunofluorescence (ii) of RAW 264.7 macrophages cultured with 1000 μg/mL n-nHA for 3 days. STXBP6 (red), nuclei (DAPI, blue). Black scale bars, 20 μm. White scale bars, 10 μm. (**B**) The distribution (i) and average (ii) of macrophage area counted from images of three independent wells. (iii) Quantitative real-time polymerase chain reaction (qPCR) analysis of *Stxbp6* gene expression in RAW 264.7 macrophages cocultured with n-nHA for 3 days. (**C**) Proliferation of 4T1 tumor cells cultured in macrophage/n-nHA-conditioned medium with n-nHA treatment (MnCM@n-nHA) or pure macrophage-conditioned medium (CM) alone for 3 days, as determined by CCK-8 assay. $^{**}P < 0.01$, $^{***}P < 0.001$.

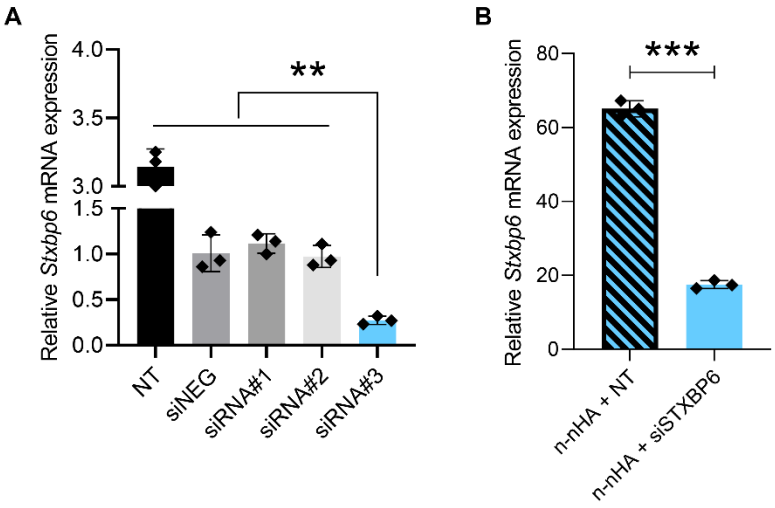

Fig. S21. siRNA screening for *Stxbp6* knockdown. (**A**) Quantitative real-time polymerase chain reaction (qPCR) analysis of *Stxbp6* gene expression in RAW264.7 macrophages transfected with no siRNA treatment (NT), negative siRNA (siNEG), candidate siRNA sequence 1 (siRNA#1), candidate siRNA sequence 2 (siRNA#2) and candidate siRNA sequence 3 (siRNA#3) at 50 nM for 2 days. (**B**) qPCR analysis examining *Stxbp6* gene expression in n-nHA-treated macrophages transfected with no siRNA treatment (NT + n-nHA) and siRNA with the maximal knockdown rate of *Stxbp6* selected above (siSTXBP6 + n-nHA). $^{**}P < 0.01$, $^{***}P < 0.001$.

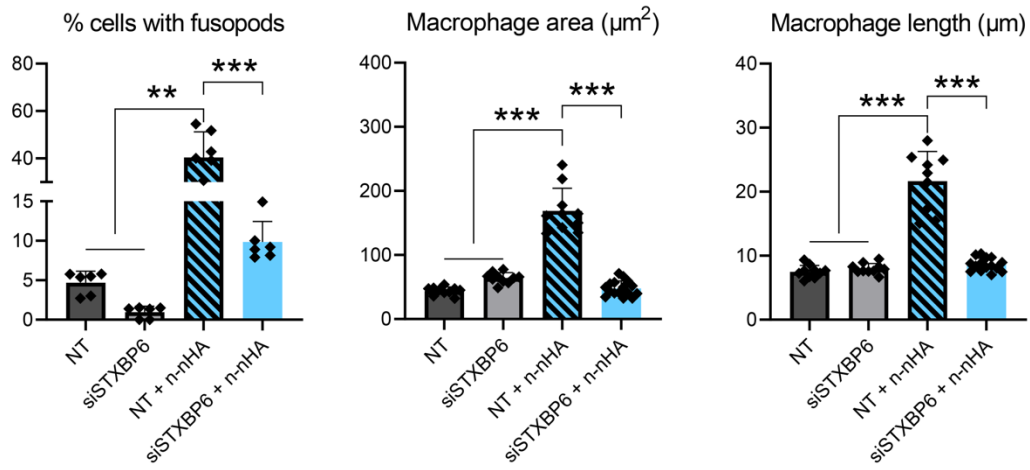

Fig. S22. *Stxbp6*-knockdown macrophages cocultured with n-nHA. The ratio of macrophges with fusopods and the quantification of macrophage area and length. NT: no siRNA treatment. siSTXBP6: siSTXBP6 treatment alone. NT + n-nHA: no siRNA treatment with n-nHA injection. siSTXBP6 + n-nHA: siSTXBP6 treatment with n-nHA injection. $^{**}P < 0.01$, $^{***}P < 0.001$.

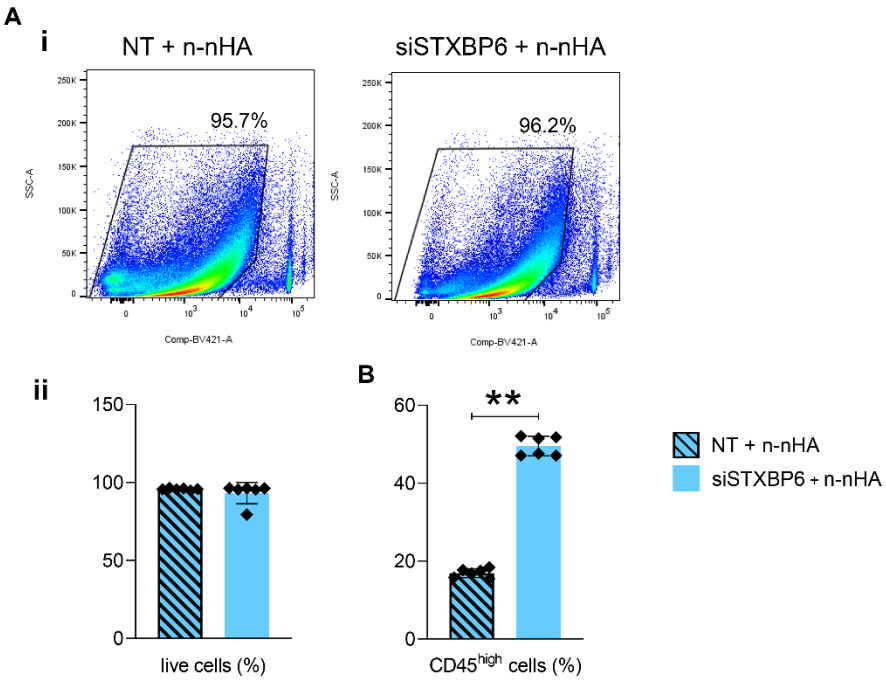

Fig. S23. Live cells and lymphocytes in the mouse tumors within a *Stxbp6*-silenced condition. (**A**) Representative scatter plots and quantification of live cells in the tumors excised at day 28. (**B**) Quantification of $CD45^{high}$ lymphocytes. $^{**}P < 0.01$. NT + n-nHA: no siRNA treatment with n-nHA injection. siSTXBP6 + n-nHA: siSTXBP6 treatment with n-nHA injection.

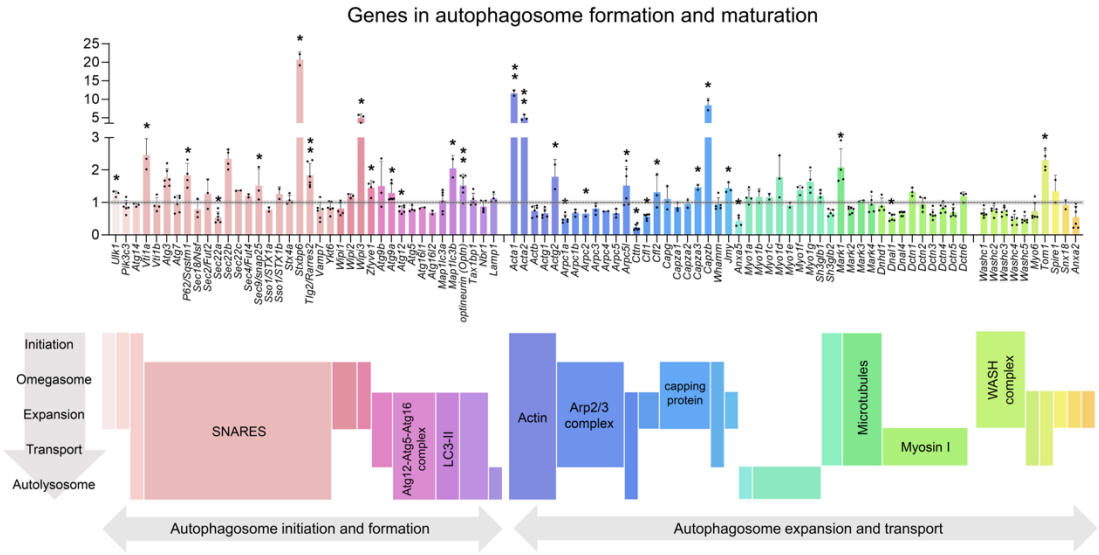

Fig. S24. Transcriptomic analysis shows that substantial n-nHA, n-gHA and n-SiO_2 (antitumor groups) significantly upregulated the expression of genes involved in various stages of autophagosome formation and maturation compared to the Ctrl group. Fold change of genes involved in various stages of autophagosome formation and maturation in antitumor groups relative to the Ctrl. The roles of these genes are distinguished by color and provided below. **P* < 0.05.

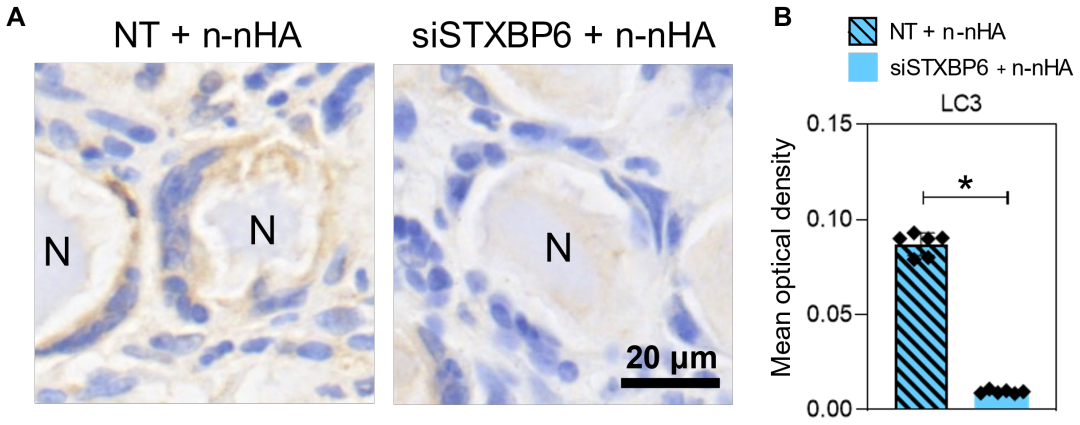

Fig. S25. *Stxbp6* knockdown impaired the high expression of LC3 induced by n-nHA. (**A**) Representative IHC images of LC3 in n-nHA-treated tumor tissues injected with siSTXBP6. Scale bar, 20 μm. (**B**) The corresponding quantification of LC3 expression. *****$P < 0.05$. NT + n-nHA: no siRNA treatment with n-nHA injection. siSTXBP6 + n-nHA: siSTXBP6 treatment with n-nHA injection.

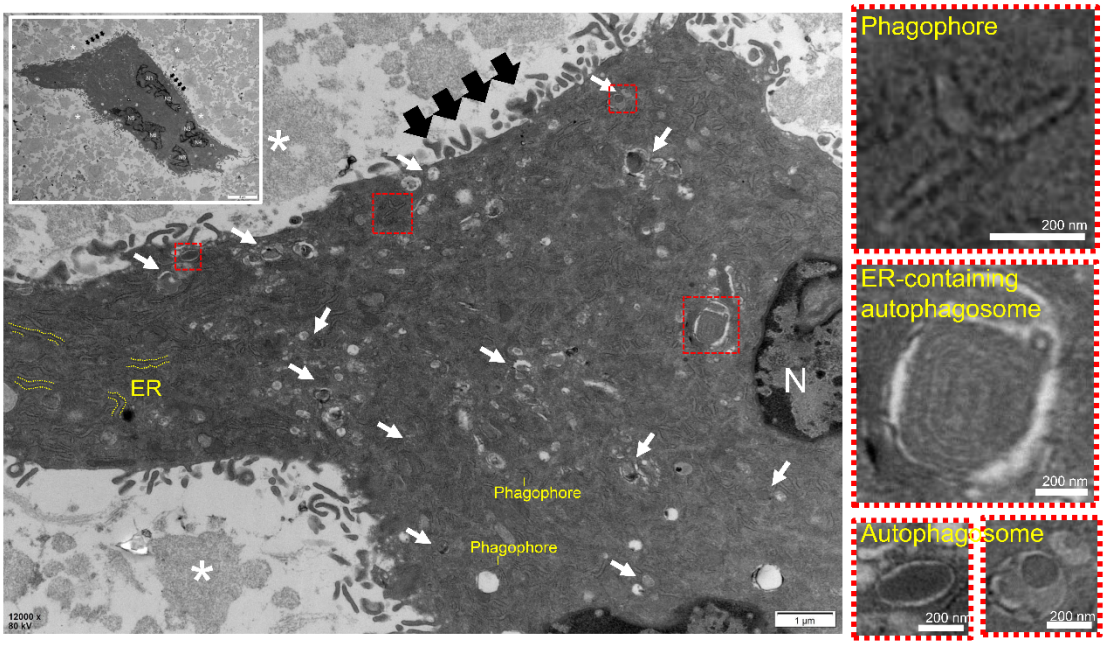

Fig. S26. Ultrastructure of multinucleated giant cell (MNGC) in tumor microenvironment treated with n-nHA. Electron micrograph of MNGC with 6 nuclei in tumor microenvironment. Cell surface presents numerous microvilli (black arrows). Cytoplasm contains numerous autophagosomes (white arrows) derived from endoplasmic reticula (ER). N, nucleus. Asterisks, n-nHA aggregates. Scale bar in left, 1 µm. Scale bars in right, 200 nm.

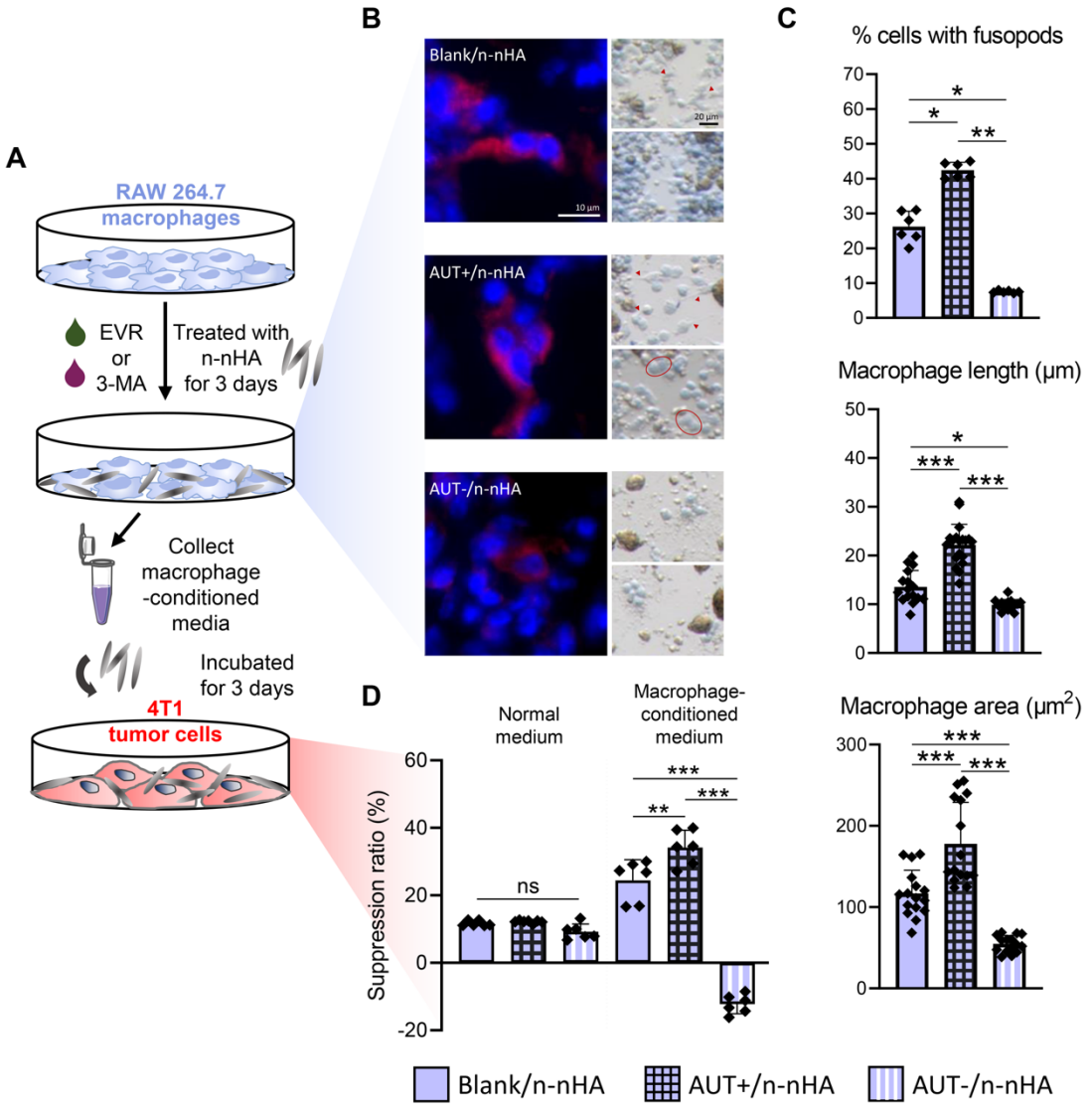

Fig. S27. The effect of autophagy on macrophage fusion and antitumor ability induced by n-nHA. (**A**) Experimental scheme for the *in vitro* antitumor assay with autophagy promotion via everolimus (EVR) or autophagy inhibition via 3-methyladenine (3-MA). EVR (0.1 μg/mL) or 3-MA (0.75 mg/mL) was added to the macrophage/n-nHA coculture system. Three days later, the obtained conditioned medium was applied to culture 4T1 tumor cells. (**B**) Representative immunofluorescence (left) and photographs (right) of n-nHA-treated macrophages incubated with EVR or 3-MA. STXBP6 (red), nuclei (DAPI, blue). White scale bar, 10 μm. Black scale bar, 20 μm. (**C**) The ratio of macrophges with fusopods and the quantification of macrophage area and length. (**D**) The suppression ratios of tumor cells cultured in normal medium and macrophage/n-nHA-conditioned medium (MnCM) of the blank/n-nHA, AUT+/n-nHA and AUT-/n-nHA groups. Blank/n-nHA: n-nHA treatment with vehicle PBS injection. AUT+/n-nHA: n-nHA treatment with EVR injection. AUT-/n-nHA: n-nHA treatment with 3-MA injection. *$P < 0.05$, **$P < 0.01$, ***$P < 0.001$.

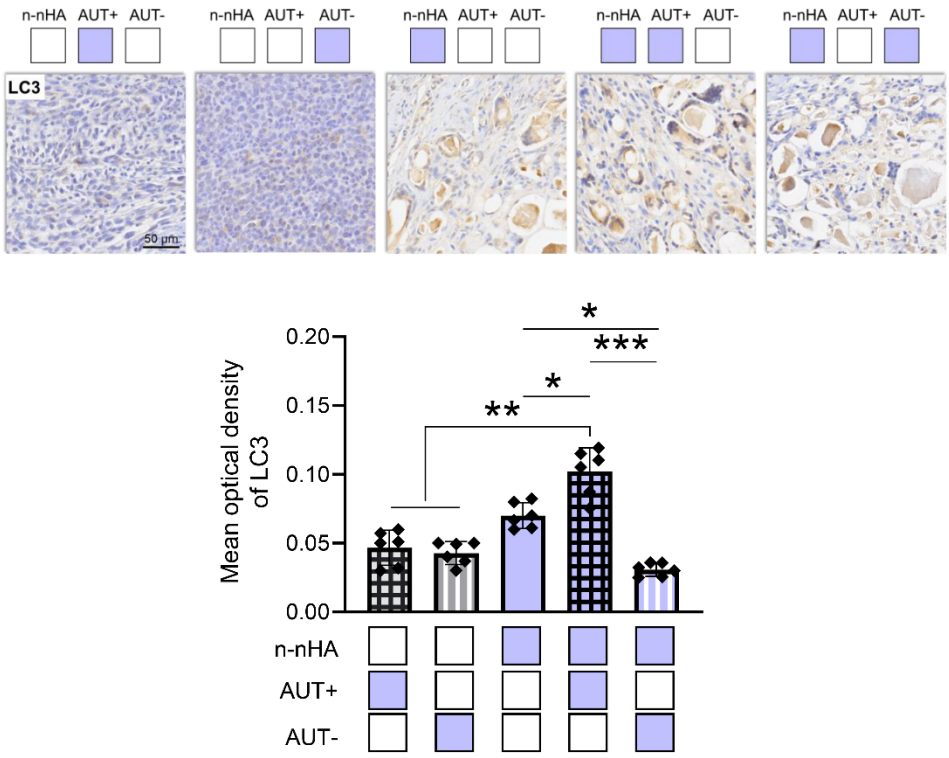

Fig. S28. Immunohistochemistry (IHC) analysis shows that the alteration of autophagy indeed affects the expression of LC3. Representative IHC images and quantification of LC3 expression in tumor tissues excised at day 28. Scale bar, 50 μm. *****$P < 0.05$, ******$P < 0.01$, *******$P < 0.001$.

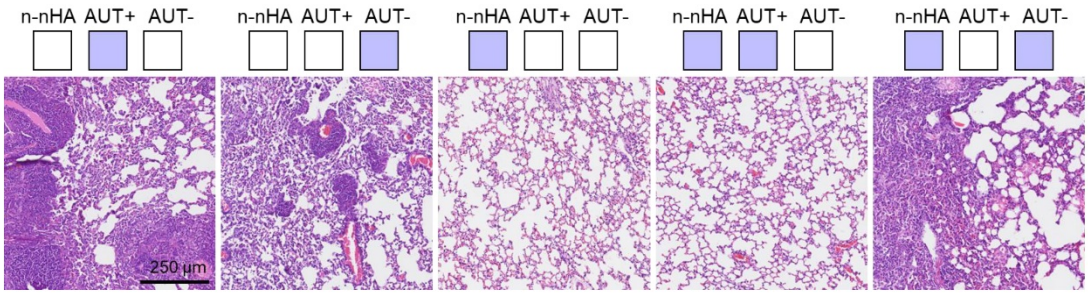

Fig. S29. H&E staining of lung tissues of tumor-bearing mice promoted or inhibited autophagy. Representative H&E staining images of lung tissues excised at day 28. Scale bar, 250 μm.

Table S1. Primer sequences used for quantitative real-time polymerase chain reaction (qPCR).

Gene	5′ to 3′	Primers
Gapdh$_{\text{mouse}}$	forward	CAC TGA GCA AGA GAG GCC CTA T
	reverse	GCA GCG AAC TTT ATT GAT GGT ATT
Cd200$_{\text{mouse}}$	forward	CTC TCC ACC TAC AGC CTG ATT
	reverse	AGA ACA TCG TAA GGA TGC AGT TG
Aebp1$_{\text{mouse}}$	forward	TTG GAA ACG CTG GAT CGG TTA
	reverse	CTT GAC CTT GCC AGG CAT TT
Jam3$_{\text{mouse}}$	forward	TCT CAA ATC CAG CAA CCG AAA C
	reverse	GTC CGT AAT GAT GCA AGA CAA T
Plpp3$_{\text{mouse}}$	forward	GCA TCA AGT ATC CCC TGA AAG TC
	reverse	CAT ACG GGT TCT GAG TGG TGG A
Stxbp6$_{\text{mouse}}$	forward	CTC TTG ATG AAA GAA TGC TGG GA
	reverse	TGA CCT TCG TGA TAG ATG CCT
Smpdl3b$_{\text{mouse}}$	forward	CAG GGG CTC AAC TAG GGA G
	reverse	GGG CCA GCA TTT AGC ACA G
Cxcl12$_{\text{mouse}}$	forward	ACC TCG GTG TCC TCT TGC TG
	reverse	CGT TGG CTC TGG CGA TGT G
Tslp$_{\text{mouse}}$	forward	CAG GCG ACA GCA TGG TTC TT
	reverse	GGC AGC CAG GGA TAG GAT TG